Lie group analysis of a pressure-driven heat and mass transport flow in an inclined magnetic field with a permeable surface

O.K. Onanuga[a], J.B. Oyetola[b] A.A.Amalare[a]
[a]Department of Physical sciences, Lagos State Polytechnic, Ikorodu, Nigeria.
[b]Department of Electrical Engineering, Lagos State Polytechnic, Ikorodu, Nigeria.
Corresponding author email: onanuga.olutayo@gmail.com

Abstract
The study investigates a convective heat and mass transfer of pressure-driven hydromagnetic flow past a fixed permeable surface in the presence of an inclined uniform magnetic field. The Newtonian fluid is influenced by pressure as well as thermal and mass convection in an isothermal system. The governing partial derivative formulated equations are reduced to a system of coupled quasilinear ordinary derivative equations using a scaling Lie group of transformations. Besides,the dimensionless derivative equations are solved analytically using the weighted residual method and the results are validated by comparing it with the shooting technique coupled with the Runge-Kutta scheme of fourth-order. The results obtained are presented graphically to characterise the effect of different relevant parameters on the dimensionless flow rate, temperature, mass species, and pressure drop. Inaddition, the effects of Skin friction, Nusselt, and Sherwood numbers are also considered and discussed. The study revealed that the pressure fields are significantly influenced by the fluid thermo-physical parameters. The mass transfer considerably changes as the heat distribution is enhanced. Also, increasing the angle of inclination of the magnetic field is observed to strongly influence the flow rate and pressure field.

Keywords: Hydromagnetic; Pressure-driven flow; Porous sheet; Lie group; Weighted residual methods.

1 Introduction

Magnetohydrodynamics (MHD) deals with the collective effects of electromagnetic forces and conducting fluid mechanical. It is the study of the magnetic properties and the behaviour of electrically conducting fluids such as liquid metals, plasmas, and electrolytes or saltwater [1]. The fundamental concept of magnetohydrodynamics is that magnetic field stimulates currents in a flowing conductive fluid,which in turn polarizes the fluid and jointly changes the magnetic field on the fluid. A pressure-driven flow of heat and mass transfer in MHD flow past a stretching permeable surface is being studied widely due to its importance in MHD power generators, reducing drag, MHD pumps, petroleum reservoirs, nuclear waste disposal, chemical catalytic reactor, Aeronautical engineering fields, and others [2,3]. As a result, its applications, Youssef et al. [4] reported on two-dimensional viscous fluid flow past slowly expanding or contracting walls with weak permeability by using the Lie-group method. They neglected the magnetic terms and pressure gradient in their analysis while Mohammad et al. [5] examined the Viscous flow through expanding or contracting gaps by permeable walls using the Optimal

Homotopy Asymptotic method. Magnetic terms were neglected but considered the effect of Reynolds number on the pressure distribution. An analytical analysis was carried out on the steady Magnetohydrodynamic Poiseuille flow through two infinite parallel porous plates in an inclined magnetic field with a constant pressure gradient by Manyonge et al. [6]. It was found that the velocity decreases in the presence of suction/injection rates, inclined magnetic field, Hartmann number, and pressure gradient. Moreso, the study of boundary layer flow of a non-Newtonian power-law fluid flow in a convergent conduit was investigated by Pramanik [7]. Magnetic terms and pressure gradient was ignored while the partial differential equations governing the problem was reduced to nonlinear differential equations using a scaling group of transformations. The cited authors above did not consider the effects of heat and mass transfer on fluid flow.

The problem of free convection under the influence of a magnetic field has attracted the mind of many scholars due to its applications in astrophysics and geophysics. As such, [8,9] carried out an analysis on MHD boundary layer flow with heat and mass transport over a moving vertical plate in the occurrence of a magnetic field with convective heat exchange at the surface as well as the surrounding while Uwanta and Sarki [10] studied heat and mass transfer by variable temperature as well as exponential mass diffusion but both authors neglected the effect of the pressure gradient in their study. Alireza et al. [11] reported on the problem of steady two-dimensional MHD stagnation point flow near a permeable stretching sheet and chemical reaction. The problem was solved analytically using the Optimal Homotopy Asymptotic method and the results compared with the fourth-order Runge-Kutta method. The study carried out in [12,13] investigated heat and mass transfer of an MHD free convection flow through a stretching sheet, chemical reaction, radiation, and heat generation in the presence of a transfer magnetic field. The problem under consideration was transformed using a similarity solution and solved by applying Nachtsheim Swigert shooting technique along with a sixth-order Runge-Kutta integration scheme. Scaling transformation for heat and mass transfer on steady MHD free convection dissipative flow past an inclined porous surface was examined by Reddy [14]. The results show that the velocity increases as thermal Grashof numbers but decreases with an increase in Prandtl and Schmidt numbers. Fatunmbi and Fenuga [15] examined MHD micropolar fluid flow over a permeable stretching sheet in the presence of variable viscosity and thermal conductivity with Soret and Dufour Effects, while Adeniyan and Adigun [16] reported on stress-work and chemical reaction effects on MHD forced convection heat and mass transfer slip-flow towards a convectively heated plate in a non-Darcian porous medium with surface mass-flux. However, the pressure, heat source, and reaction rate terms were not taken into account in the study.

The pressure-driven flow of magnetohydrodynamics heat and mass transfer problems are important in many engineering processes and has received considerable attention from many researchers in recent years. In processes such as fluid droplet sprays, purification of crude oil, flow in a desert cooler, energy transfer in a wet cooling tower, and possible applications in many industries, Salawu et al. [17]. For example, the water industry, petroleum industry, drilling industry, sewage treatment industry, and many more. Time-dependent pressure gradient influence on unsteady MHD Couette flow and heat transfer of a Casson fluid was analyzed by Sayed-Ahmed et al. [18]. The fluid was influenced by a regular and exponential decaying pressure gradient, an external uniform magnetic field is applied perpendicular to the plates with the fluid motion subjected to a uniform injection and suction, while Farooq et al. [19] examined steady Poiseuille flow and heat transfer of couple stress fluids between two parallel inclined

plates with variable viscosity. Reynold's model for temperature-dependent viscosity was used. Thiagarajan and Sangeetha [20] reported on nonlinear MHD boundary layer fluid flow with heat transfer through a stretching plate and free stream pressure gradient in the existence of variable viscosity and thermal conductivity.
The above studies cited, neglected the influence of the inclined magnetic field and the effects of some fluid parameters on the fluid pressure. The present study investigates the combined effects of an inclined magnetic field and pressure drop in a steady convective heat and mass transfer of magnetohydrodynamic flow. The flow is pressure-driven past a fixed permeable surface with the inclined uniform magnetic field. To achieve the aims of this study, Lie group transformation was applied to reduce the system of partial differential equations to a system of ordinary differential equations by reducing the number of independent variables. The weighted residual method was used to obtain the solution of the non-linear differential equations governing the fluid flow problem.

2 Formulation of the problem

An investigation was carried out to examine free convective heat and mass transfer of two-dimensional MHD pressure-driven flow of an electrically conducting, steady, viscous, laminar, and incompressible fluid flow past a permeable plate under the influence of uniform inclined magnetic field and pressure gradient. The motion of the fluid is maintained by both pressure gradient and gravity, and the flow is assumed to be in the X-direction with Y-axis normal to it. The magnetic field of uniform strength B_0 is introduced at angle α lying in the range $0 \prec \alpha \prec \frac{\pi}{2}$ in the direction of the flow. The plate is maintained at the temperature and species concentration T_w, C_w and free stream temperature and species concentration T_∞, C_∞ respectively. The geometry and equations governing the steady heat and mass transfer of two-dimensional magnetohydrodynamic Poiseuille fluid flow past a permeable plate with an inclined magnetic field are as follows:

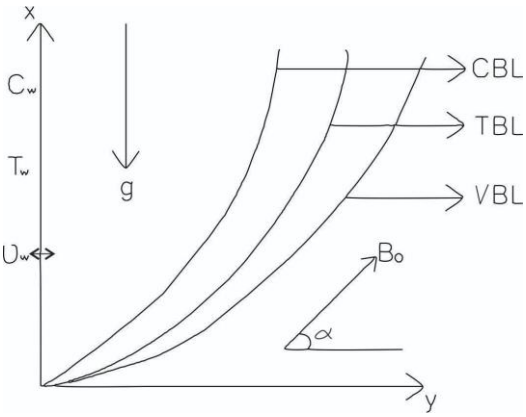

Figure 1: The flow coordinate

$$\frac{\partial U}{\partial X} + \frac{\partial V}{\partial Y} = 0 \tag{1}$$

$$U\frac{\partial U}{\partial X} + V\frac{\partial U}{\partial Y} = -\frac{1}{\rho}\sigma B_0^2 U sin^2\alpha - \frac{1}{\rho}\frac{\partial P}{\partial X} + \nu\left(\frac{\partial^2 U}{\partial X^2} + \frac{\partial^2 U}{\partial Y^2}\right) + g\beta_T(T - T_\infty) + g\beta_C(C - C_\infty) \tag{2}$$

$$U\frac{\partial V}{\partial X}+V\frac{\partial V}{\partial Y}=-\frac{1}{\rho}\frac{\partial P}{\partial Y}+\nu\left(\frac{\partial^2 V}{\partial X^2}+\frac{\partial^2 V}{\partial Y^2}\right)-\frac{1}{\rho}\sigma B_0^2 V sin^2\alpha \quad (3)$$

$$\rho C_p\left(U\frac{\partial T}{\partial X}+V\frac{\partial T}{\partial Y}\right)=k\left(\frac{\partial^2 T}{\partial X^2}+\frac{\partial^2 T}{\partial Y^2}\right)+Q_0(T-T_\infty) \quad (4)$$

$$U\frac{\partial C}{\partial X}+V\frac{\partial C}{\partial Y}=D\left(\frac{\partial^2 C}{\partial X^2}+\frac{\partial^2 C}{\partial Y^2}\right)-\gamma(C-C_\infty) \quad (5)$$

The initial and boundary conditions are as follows:

$$\begin{aligned} &U=0, V=v_w, P=0, T=T_\infty+(T_w-T_\infty)AX, C=C_\infty+(C_w-C_\infty)BX \quad at \quad Y=0 \\ &U=0, T=T_\infty, C=C_\infty \quad as \quad Y\to\infty \end{aligned} \quad (6)$$

Using the following non-dimensional quantities

$$\begin{aligned} &x=\frac{X}{l}, y=\frac{Y}{l}, u=\frac{Ul}{\nu}, v=\frac{Vl}{\nu}, p=\frac{Pl^2}{\rho\nu^2}, H_a=lB_0\sqrt{\frac{\sigma}{\mu}}, \theta=\frac{T-T_\infty}{T_w-T_\infty}, P_r=\frac{\mu C_p}{k}, \\ &S_c=\frac{\nu}{D}, G_r=\frac{l^3 g\beta_T(T_w-T_\infty)}{\nu^2}, G_c=\frac{l^3 g\beta_C(C_w-C_\infty)}{\nu^2}, \phi=\frac{C-C_\infty}{C_w-C\infty}, \lambda=\frac{l^2\gamma}{\nu}, \\ &Q=\frac{l^2 Q_0}{\mu C_p}, f_w=-\frac{v_w l}{\nu} \end{aligned} \quad (7)$$

Substituting (7) into equation (1)-(6), to obtain

$$\frac{\partial u}{\partial x}+\frac{\partial v}{\partial y}=0 \quad (8)$$

$$u\frac{\partial u}{\partial x}+v\frac{\partial u}{\partial y}=-H_a^2 u sin^2\alpha-\frac{\partial p}{\partial x}+\left(\frac{\partial^2 u}{\partial x^2}+\frac{\partial^2 u}{\partial y^2}\right)+G_r\theta+G_c\phi \quad (9)$$

$$\frac{\partial v}{\partial x}+v\frac{\partial v}{\partial y}=-\frac{\partial p}{\partial y}+\left(\frac{\partial^2 v}{\partial x^2}+\frac{\partial^2 v}{\partial y^2}\right)-H_a^2 v sin^2\alpha \quad (10)$$

$$u\frac{\partial \theta}{\partial x}+v\frac{\partial \theta}{\partial y}=\frac{1}{P_r}\left(\frac{\partial^2 \theta}{\partial x^2}+\frac{\partial^2 \theta}{\partial y^2}\right)+Q\theta \quad (11)$$

$$u\frac{\partial \phi}{\partial x}+v\frac{\partial \phi}{\partial y}=\frac{1}{S_c}\left(\frac{\partial^2 \phi}{\partial x^2}+\frac{\partial^2 \phi}{\partial y^2}\right)-\lambda\phi \quad (12)$$

The corresponding initial and boundary conditions become:

$$\begin{aligned} &u=0, v=-f_w, p=0, \theta=x, \phi=x \quad at \quad y=0 \\ &u=0, \theta=0, \phi=0 \quad as \quad y\to\infty \end{aligned} \quad (13)$$

Introducing the stream function $u=\frac{\partial \psi}{\partial y}$, $v=-\frac{\partial \psi}{\partial x}$, the continuity equation is satisfied and equations (9)-(13), gives

$$\frac{\partial \psi}{\partial y}\frac{\partial^2 \psi}{\partial x\partial y}-\frac{\partial \psi}{\partial x}\frac{\partial^2 \psi}{\partial y^2}=-H_a^2 sin^2\alpha\left(\frac{\partial \psi}{\partial y}\right)-\frac{\partial p}{\partial x}+\left(\frac{\partial^3 \psi}{\partial x^2\partial y}+\frac{\partial^3 \psi}{\partial y^3}\right)+G_r\theta+G_c\phi \quad (14)$$

$$-\frac{\partial \psi}{\partial y}\frac{\partial^2 \psi}{\partial x^2}+\frac{\partial \psi}{\partial x}\frac{\partial^2 \psi}{\partial x\partial y}=-\frac{\partial p}{\partial y}-\left(\frac{\partial^3 \psi}{\partial x^3}+\frac{\partial^3 \psi}{\partial x\partial y^2}\right)+H_a^2 sin^2\alpha\left(\frac{\partial \psi}{\partial x}\right) \quad (15)$$

$$\frac{\partial \psi}{\partial y}\frac{\partial \theta}{\partial x}-\frac{\partial \psi}{\partial x}\frac{\partial \theta}{\partial y}=\frac{1}{P_r}\left(\frac{\partial^2 \theta}{\partial x^2}+\frac{\partial^2 \theta}{\partial y^2}\right)+Q\theta \quad (16)$$

$$\frac{\partial\psi}{\partial y}\frac{\partial\phi}{\partial x}-\frac{\partial\psi}{\partial x}\frac{\partial\phi}{\partial y}=\frac{1}{S_c}\left(\frac{\partial^2\phi}{\partial x^2}+\frac{\partial^2\phi}{\partial y^2}\right)-\lambda\phi \tag{17}$$

subject to the initial and boundary conditions

$$\begin{aligned}&\frac{\partial\psi}{\partial y}=0,\frac{\partial\psi}{\partial x}=f_w,p=0,\theta=x,\phi=x \quad at \quad y=0\\&\frac{\partial\psi}{\partial y}=0,\theta=0,\phi=0 \quad as \quad y\to\infty\end{aligned} \tag{18}$$

Introducing a simplified form of Lie-group transformations namely, the scaling group of transformations to equations (14)-(18) is equivalent to determining the invariant solutions of these equations under a continuous one-parameter group [21-23]. One of the methods is to search for a transformation group from an elementary set of one-parameter scaling group of transformations, given as ∇

$$\begin{aligned}&\nabla: x^*=xe^{\epsilon\alpha_1},y^*=ye^{\epsilon\alpha_2},\psi^*=\psi e^{\epsilon\alpha_3},u^*=ue^{\epsilon\alpha_4},v^*=ve^{\epsilon\alpha_5},\\&p^*=pe^{\epsilon\alpha_6},\theta^*=\theta e^{\epsilon\alpha_7},\phi^*=\phi e^{\epsilon\alpha_8}\end{aligned} \tag{19}$$

where α_1, α_2, α_3, α_4, α_5, α_6, α_7, and α_8, are transformation parameters of the group to be determined later and ϵ is a small parameter. Equation (19) may be considered as a point-transformation which transforms coordinate $(x,y,\psi,u,v,\theta,\phi)$ to the coordinate $(x^*,y^*,\psi^*,u^*,v^*,\theta^*,\phi^*)$.

The task is to find relationships among the exponents $\alpha's$ such that Equations (14)-(18) will remain invariant under the point transformations. Substituting transformation (19) into Equations (14)-(18) and applying invariant conditions yields

$$\alpha_1=\alpha_3=\alpha_4=\alpha_7=\alpha_8,\alpha_3=\frac{1}{2}\alpha_1,\alpha_2=\alpha_5=\alpha_6=0 \tag{20}$$

Thus the set of transformations ∇ reduces to a one-parameter group of transformations as

$$x^*=xe^{\epsilon\alpha_1},y^*=y,\psi^*=\psi e^{\epsilon\alpha_1},u^*=ue^{\epsilon\alpha_1},v^*=v,p^*=p,\theta^*=\theta e^{\epsilon\alpha_1},\phi^*=\phi e^{\epsilon\alpha_1} \tag{21}$$

Finding the absolute invariant, the similarity transformations is obtained as:

$$\eta=y,\psi=xf(\eta),p=p_d(\eta),\theta=x\theta(\eta),\phi=x\phi(\eta) \tag{22}$$

Substituting the similarity variables (22) into equations (14)-(18). the following system of non-linear differential equations is obtained.

$$f'''+ff''-f'^2-M^2f'+G_r\theta+G_c\phi=0 \tag{23}$$

$$-p_d'=f''+ff'+M^2f' \tag{24}$$

$$\theta''+P_rf\theta'-P_rf'\theta+P_rQ\theta=0 \tag{25}$$

$$\phi''+S_cf\phi'-S_cf'\phi-S_c\lambda\phi=0 \tag{26}$$

The corresponding initial and boundary conditions take the form:

$$\begin{aligned}&f=f_w,f'=0,p_d=0,\theta=1,\phi=1 \quad at \quad \eta=0\\&f'=0,\theta=0,\phi=0 \quad at \quad \eta\to\infty\end{aligned} \tag{27}$$

Integrating equation (24) with the initial and boundary conditions when $f_w=1$, let pressure drop $-p_d=G$, this becomes

$$G = f' + \frac{1}{2}f^2 - (\frac{1}{2} + M^2) + M^2 f \tag{28}$$

3 Weighted Residual Method

The idea of a weighted residual method [23-26] is to seek an approximate solution, in form of a polynomial to the differential equation of the form

$$L[u(x)] = f \quad in \quad the \quad domain \quad T, \qquad B_\mu[u] = \gamma_\mu \quad on \quad \partial T \tag{29}$$

where $L[u]$ denotes a differential operator linear or non-linear involving spatial derivatives of dependent variables u, f is known to function of position, $B_\mu[u]$ represents the approximate number of boundary conditions and T is the domain with boundary ∂T.

Applying WRM to equations (23)-(28). We assume a polynomial with unknown coefficients or parameters to be determined later, this polynomial is called the trial function.

$$f(\eta) = \sum_{i=0}^{n} a_i \eta^i, \qquad \theta(\eta) = \sum_{i=0}^{n} b_i \eta^i, \qquad \phi(\eta) = \sum_{i=0}^{n} c_i \eta^i \tag{30}$$

Impose the boundary conditions on the trial functions also substituting the trial functions into equations (23), (25), and (26) to obtain the residuals

$$\begin{aligned} f_r = \; & 6a_3 + 24a_4\eta + 60a_5\eta^2 + 120a_6\eta^3 + 210a_7\eta^4 + 336a_8\eta^5 + 504a_9\eta^6 + 720a_{10}\eta^7 \\ & +990a_{11}\eta^8 + 1320a_{12}\eta^9 + (a_{12}\eta^{12} + a_{11}\eta^{11} + a_{10}\eta^{10} + a_9\eta^9 + a_8\eta^8 + a_7\eta^7 \\ & +a_6\eta^6 + a_5\eta^5 + a_4\eta^4 + a_3\eta^3 + a_2\eta^2 + a_1\eta + a_0)(132a_{12}\eta^{10} + 110a_{11}\eta^9 \\ & +90a_{10}\eta^8 + 72a_9\eta^7 + 56a_8\eta^6 + 42a_7\eta^5 + 30a_6\eta^4 + 20a_5\eta^3 + 12a_4\eta^2 + 6a_3\eta + 2a_2) \\ & -(12a_{12}\eta^{11} + 11a_{11}\eta^{10} + 10a_{10}\eta^9 + 9a_9\eta^8 + 8a_8\eta^7 + 7a_7\eta^6 + 6a_6\eta^5 + 5a_5\eta^4 \\ & +4a_4\eta^3 + 3a_3\eta^2 + 2a_2\eta + a_1)^2 - -H_a^2 sin^2\alpha(12a_{12}\eta^{11} + 11a_{11}\eta^{10} + 10a_{10}\eta^9 + 9a_9\eta^8 \\ & +8a_8\eta^7 + 7a_7\eta^6 + 6a_6\eta^5 + 5a_5\eta^4 + 4a_4\eta^3 + 3a_3\eta^2 + 2a_2\eta + a_1) + G_r(b_{12}\eta^{12} \\ & +b_{11}\eta^{11} + b_{10}\eta^{10} + b_9\eta^9 + b_8\eta^8 + b_7\eta^7 + b_6\eta^6 + b_5\eta^5 + b_4\eta^4 + b_3\eta^3 + b_2\eta^2 \\ & +b_1\eta + b_0) + G_c(c_{12}\eta^{12} + c_{11}\eta^{11} + c_{10}\eta^{10} + c_9\eta^9 + c_8\eta^8 + c_7\eta^7 + c_6\eta^6 + c_5\eta^5 \end{aligned} \tag{31}$$

$$\begin{aligned} \theta_r = \; & 2b_2 + 6b_3\eta + 12b_4\eta^2 + 20b_5\eta^3 + 30b_6\eta^4 + 42b_7\eta^5 + 56b_8\eta^6 + 72b_9\eta^7 + 90b_{10} \\ & \eta^8 + 110b_{11}\eta^9 + 132b_{12}\eta^{10} + P_r(a_{12}\eta^{12} + a_{11}\eta^{11} + a_{10}\eta^{10} + a_9\eta^9 + a_8\eta^8 + a_7\eta^7 \\ & +a_6\eta^6 + a_5\eta^5 + a_4\eta^4 + a_3\eta^3 + a_2\eta^2 + a_1\eta + a_0)(12b_{12}\eta^{11} + 11b_{11}\eta^{10} + 10b_{10}\eta^9 \\ & +9b_9\eta^8 + 8b_8\eta^7 + 7b_7\eta^6 + 6b_6\eta^5 + 5b_5\eta^4 + 4b_4\eta^3 + 3b_3\eta^2 + 2b_2\eta + b_1) \\ & -P_r(12a_{12}\eta^{11} + 11a_{11}\eta^{10} + 10a_{10}\eta^9 + 9a_9\eta^8 + 8a_8\eta^7 + 7a_7\eta^6 + 6a_6\eta^5 + 5a_5\eta^4 \\ & +4a_4\eta^3 + 3a_3\eta^2 + 2a_2\eta + a_1)(b_{12}\eta^{12} + b_{11}\eta^{11} + b_{10}\eta^{10} + b_9\eta^9 + b_8\eta^8 \\ & +b_7\eta^7 + b_6\eta^6 + b_5\eta^5 + b_4\eta^4 + b_3\eta^3 + b_2\eta^2 + b_1\eta + b_0) + P_rQ(b_{12}\eta^{12} + b_{11}\eta^{11} \\ & +b_{10}\eta^{10} + b_9\eta^9 + b_8\eta^8 + b_7\eta^7 + b_6\eta^6 + b_5\eta^5 + b_4\eta^4 + b_3\eta^3 + b_2\eta^2 \\ & +b_1\eta + b_0) \end{aligned} \tag{32}$$

$$\begin{aligned}\phi_r = \; & 2c_2 + 6c_3\eta + 12c_4\eta^2 + 20c_5\eta^3 + 30c_6\eta^4 + 42c_7\eta^5 + 56c_8\eta^6 + 72c_9\eta^7 + 90c_{10}\eta^8 \\ & +110c_{11}\eta^9 + 132c_{12}\eta^{10} + S_c(a_{12}\eta^{12} + a_{11}\eta^{11} + a_{10}\eta^{10} + a_9\eta^9 + a_8\eta^8 + a_7\eta^7 \\ & +a_6\eta^6 + a_5\eta^5 + a_4\eta^4 + a_3\eta^3 + a_2\eta^2 + a_1\eta + a_0)(12c_{12}\eta^{11} + 11c_{11}\eta^{10} + 10c_{10}\eta^9 \\ & +9c_9\eta^8 + 8c_8\eta^7 + 7c_7\eta^6 + 6c_6\eta^5 + 5c_5\eta^4 + 4c_4\eta^3 + 3c_3\eta^2 + 2c_2\eta + c_1) \\ & -S_c(12a_{12}\eta^{11} + 11a_{11}\eta^{10} + 10a_{10}\eta^9 + 9a_9\eta^8 + 8a_8\eta^7 + 7a_7\eta^6 + 6a_6\eta^5 + 5a_5\eta^4 \\ & +4a_4\eta^3 + 3a_3\eta^2 + 2a_2\eta + a_1)(c_{12}\eta^{12} + c_{11}\eta^{11} + c_{10}\eta^{10} + c_9\eta^9 + c_8\eta^8 + c_7\eta^7 + c_6\eta^6 \\ & +c_5\eta^5 + c_4\eta^4 + c_3\eta^3 + c_2\eta^2 + c_1\eta + c_0) - S_c\lambda(c_{12}\eta^{12}c_{11}\eta^{11} + c_{10}\eta^{10} \\ & +c_9\eta^9 + c_8\eta^8 + c_7\eta^7 + c_6\eta^6 + c_5\eta^5 + c_4\eta^4 + c_3\eta^3 + c_2\eta^2 + c_1\eta + c_0)\end{aligned} \tag{33}$$

Minimizing the residual error to zero at some set of collocation points within the domain to obtain the unknown coefficients. Substituting the obtained constant values into the trial functions to get the tangential velocity, temperature, and concentration equations respectively.

$$\begin{aligned}f(\eta) = \; & 1.000000000 + 2.099284246\eta^2 - 3.047632751\eta^3 + 2.530136157\eta^4 \\ & -1.470259657\eta^5 + 0.6293250241\eta^6 - 0.1991658321\eta^7 + 0.0454804339\eta^8 \\ & -0.0070852237\eta^9 + 0.00067064439\eta^{10} - 0.00002841484\eta^{11} \\ & -0.000000010279\eta^{12}\end{aligned} \tag{34}$$

$$\begin{aligned}\theta(\eta) = \; & 1.000000000 - 0.7501015305\eta - 0.08820358330\eta^2 + 0.6074318152\eta^3 \\ & -0.7261180797\eta^4 + 0.5709303379\eta^5 - 0.3295917512\eta^6 + 0.1429428400\eta^7 \\ & -0.04630653096\eta^8 + 0.01089292777\eta^9 - 0.001757153433\eta^{10} \\ & +0.0001735751976\eta^{11} - 0.000007901449859\eta^{12}\end{aligned} \tag{35}$$

$$\begin{aligned}\phi(\eta) = \; & 1.000000000 - 1.420604887\eta + 0.7550189757\eta^2 + 0.1114517669\eta^3 \\ & -0.5521183085\eta^4 + 0.5564172609\eta^5 - 0.3637757365\eta^6 + 0.1733374400\eta^7 \\ & -0.06091843489\eta^8 + 0.01538962724\eta^9 - 0.002639573886\eta^{10} \\ & +0.0002746098028\eta^{11} - 0.00001305341620\eta^{12}\end{aligned} \tag{36}$$

Differentiate equation (34) to obtain

$$\begin{aligned}f'(\eta) = \; & 4.198568492\eta - 9.142898253\eta^2 + 10.12054463\eta^3 - 7.351298285\eta^4 \\ & +3.775950145\eta^5 - 1.394160825\eta^6 + 0.3638434712\eta^7 - 0.0637670133\eta^8 \\ & +0.00670644390\eta^9 - 0.00031256324\eta^{10} - 0.00000123348\eta^{11}\end{aligned} \tag{37}$$

Also substituting for f and f' in (3.35) with the corresponding constant values to obtain the pressure drop as,

$$G(\eta) = -0.5000000000 - 5.919583592\eta - 9.24848031\eta^2 + 5.897473791\eta^3 - 0.7398864645\eta^4 - 1.701380258\eta^5 + 1.567161938\eta^6 - 0.7405884216\eta^7 - 0.2197160842\eta^8 - 0.04091577803\eta^9 + 0.004261080147\eta^{10} - 0.0001553604408\eta^{11} + 1/2(1.000000000 + 2.9579917960\eta^2 - 3.329319907\eta^3 + 1.682450942\eta^4 - 0.23209984000\eta^5 - 0.2738925496\eta^6 + 0.2336621536\eta^7 + 0.09987549500\eta^8 + 0.02718721756\eta^9 - 0.004771258242\eta^{10} + 0.0004958086097\eta^{11} - 0.00002327604943\eta^{12})^2 \quad (38)$$

Skin Friction

$$\tau = \frac{\partial^2 f}{\partial \eta^2} = 4.198568492 - 18.28579651\eta + 30.36163388\eta^2 - 29.40519314\eta^3 + 18.87975072\eta^4 - 8.364964948\eta^5 + 2.546904301\eta^6 - 0.5101361065\eta^7 + 0.06035799510\eta^8 - 0.003125631885\eta^9 - 0.00001356775269\eta^{10} \quad (39)$$

Nusselt Number

$$Nu = -\frac{\partial \theta}{\partial \eta} = 4.198568492\eta - 9.142898253\eta^2 + 10.12054463\eta^3 - 7.351298285\eta^4 + 3.775950145\eta^5 - 1.394160825\eta^6 + 0.3638434716\eta^7 - 0.06376701332\eta^8 + 0.006706443900\eta^9 - 0.0003125631885\eta^{10} - 0.000001233432062\eta^{11} \quad (40)$$

Sherwood Number

$$Sh = -\frac{\partial \phi}{\partial \eta} = 4.198568492\eta - 9.142898253\eta^2 + 10.12054463\eta^3 - 7.351298285\eta^4 + 3.775950145\eta^5 - 1.394160825\eta^6 + 0.3638434716\eta^7 - 0.06376701332\eta^8 + 0.006706443900\eta^9 - 0.0003125631885\eta^{10} - 0.000001233432062\eta^{11} \quad (41)$$

The process of the weighted residual method is repeated for different values of G_r, G_c, H_a, α, Q, P_r, S_c and λ. The following computational results in the table are obtained and compared with the shooting technique along with the fourth-order Runge-Kutta method.

Table 1: Comparison of τ, Nu, and Sh for various values of G_r, G_c, Q and S_c (PP-Physical Parameters)

		Weighted Residual method			4^{th} order R-K		
PP	values	τ	Nu	Sh	τ	Nu	Sh
G_r	2.5	2.86521	0.53944	1.34943	2.86359	0.53931	1.34902
	5.5	3.77012	0.69197	1.39921	3.76616	0.69173	1.39866
	7	4.19857	0.75010	1.42060	4.19315	0.74981	1.41999
G_c	4.5	3.59067	0.68694	1.39516	3.58741	0.68673	1.39467
	5.5	3.83489	0.71293	1.40549	3.83083	0.71269	1.40495
	7	4.19857	0.75010	1.42060	4.19315	0.74981	1.41998

Q	0.3	4.02001	1.08149	1.40258	4.01476	1.08098	1.40195
	1.0	4.19857	0.75010	1.42060	4.19315	0.74981	1.41998
	2.0	4.63757	0.01876	1.46429	4.63208	0.01877	1.46368
S_c	0.01	4.79802	0.93631	0.35822	4.79293	0.93598	0.35822
	0.1	4.65693	0.89254	0.56181	4.65179	0.89221	0.56179
	0.62	4.19857	0.75010	1.42061	4.193156	0.74981	1.41999

4 Results and Discussion

The numerical computation has been carried out using the Weighted Residual method for variations in the governing parameters, the Hartmann number H_a, angle of inclination α, thermal Grashof number G_r, heat source Q, Prandtl number P_r, solutal Grashof number G_c, Schmidt number S_c and reaction rate parameter λ. The following default parameter values are adopted for computation: G_r=G_c=7, Q=λ=1, P_r=0.72, S_c=0.62, H_a=5 and $\alpha = 30^0$. All graphs, therefore, match these values unless in particular indicated on the appropriate graph. Table 1 shows the effect of some parameters on skin friction, Nusselt, and Sherwood number. It clearly shows that an increase in the solutant and thermal Grashof number has an accelerating effect on the skin friction, Nusselt, and Sherwood number respectively. An increase in heat source increases skin friction and Sherwood number while it retards the Nusselt number because heat within the boundary layer reduces. Also, skin friction and Nusselt number decreases as the Schmidt number increases but have an increasing effect on the Sherwood number.

Figures 2 and 3 represent the velocity and pressure profiles for different values of Hartmann number H_a. It is found that a rise in the magnetic field parameter H_a decreases the velocity and pressure profiles. This is because the magnetic field exerts a retarding force on the convective fluid flow. A Lorentz force is induced as the magnetic term increases all over the flow regime that opposes the flow field. As magnetic values rise, the impact of Lorentz force is encouraged that in turn decreases heat source terms thereby causes the fluid to decline. Figures 4 and 5 show the velocity and pressure profiles for various angles of inclination of the magnetic field α, while other parameters are kept fixed at some values. An increase in the angle of inclination is noticed to diminish the effect of the buoyancy force and thereby the driving force of the fluid flow decreases. As a result, the velocity and pressure distributions decrease, as such pressure and flow rate are discouraged. The influence of different values of the thermal Grashof number G_r on the velocity and pressure profiles are presented in figures 6 and 7. It is observed that an increase in the values of the relative effect of the thermal buoyancy force on the viscous hydrodynamic force in the boundary layer causes an increase in the velocity and pressure distributions. The effect of variations in the ratio of the species buoyancy force to the hydrodynamic force in the boundary layer on the velocity and pressure distributions are illustrated in figures 8 and 9. The numerical results show the effect of increasing values of solutal Grashof number G_c causes an increase in the velocity and pressure distributions. This is due to rising in the heat source terms that decreases the fluid bonding force, this, therefore, enhances the sensitivity of the flow characteristics. The velocity distribution attains a maximum value and then decreases gradually towards the free stream.

Figures 10, 11, and 12 show the effect of different values of the Prandtl number P_r on the velocity, pressure, and temperature profiles. It is found that variations in the ratio of momentum diffusivity to thermal diffusivity result in a respectively decrease in velocity and pressure distributions. The figures show an increase in the values of P_r results in a decrease of the momentum, thermal, and mass boundary layers thickness and reduce the average temperature

within the boundary layers. Smaller values of P_r equivalents to an increasing in the thermal conductivity and heat is will diffuse out from the heated plate than higher values of P_r. Figures 13, 14, and 15 depict the effect of Schmidt number S_c on the velocity, pressure, and concentration profiles. Schmidt number is the ratio of the momentum to the mass diffusivity. An increase in S_c slow down the velocity, pressure, and concentration profiles which are accompanied by a simultaneous decrease in the velocity, pressure, and concentration boundary layers. Schmidt number quantifies the relative effectiveness of momentum and mass transfer through diffusion in the hydrodynamic velocity, pressure, and concentration boundary layers.
Figures 16, 17, and 18 represent the effects of the heat source parameter on the velocity, pressure, and temperature profiles. it is noticed that velocity, pressure, and temperature increase rapidly as the heat source parameter Q increases. The figures indicate that increasing heat source parameter Q, increases the momentum and thermal boundary layers thickness that in turn increases the shear stress and reduces the heat transfer coefficient at the surface respectively. Figures 19, 20, and 21 present the effects of reaction rate parameter λ on the velocity, pressure, and concentration distributions. An increase in the values of λ, decreases the velocity and pressure profiles (figures 19 and 20). From Figure 21, it is very clear that the reactive solutal profiles decrease with an increase in the values of λ, that is the reaction rate parameter is a decreasing agent and as a result, the solute boundary layer close to the wall becomes thinner. This is due to the fact the conversion of the species takes place near the wall as a result of the chemical reaction and then decrease the concentration in the boundary layer. All these agree with the expectations.

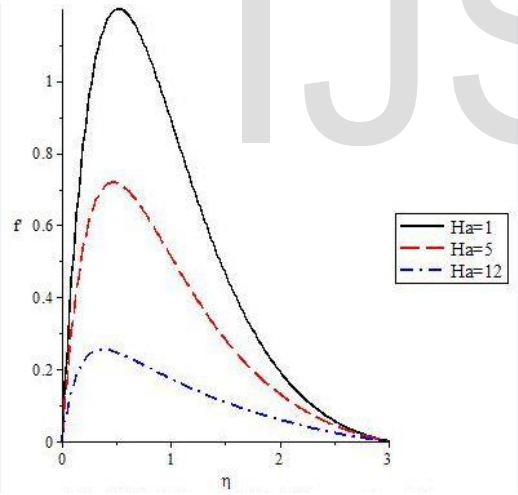

Figure 2: Velocity field for various Ha

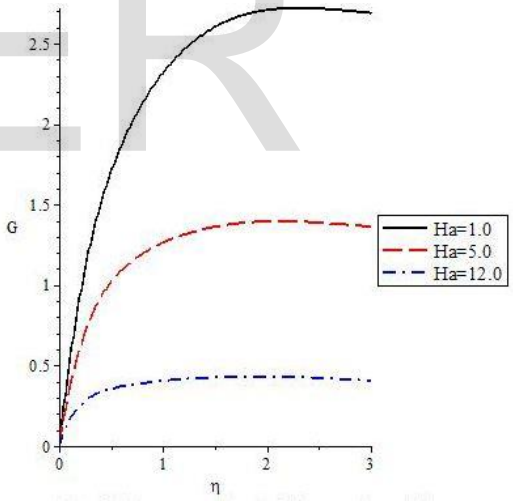

Figure 3: Pressure distribution for diverse Ha

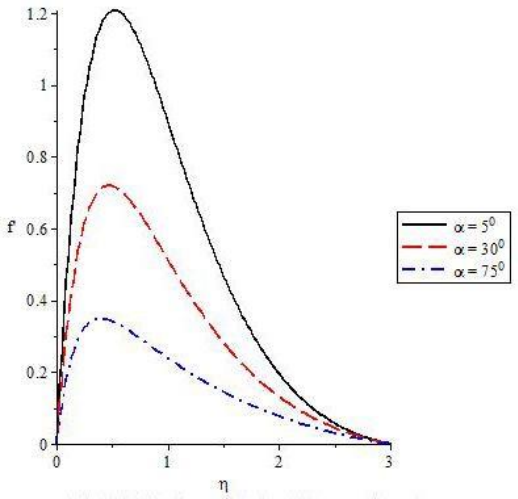

Figure 4: Flow rate at different angle

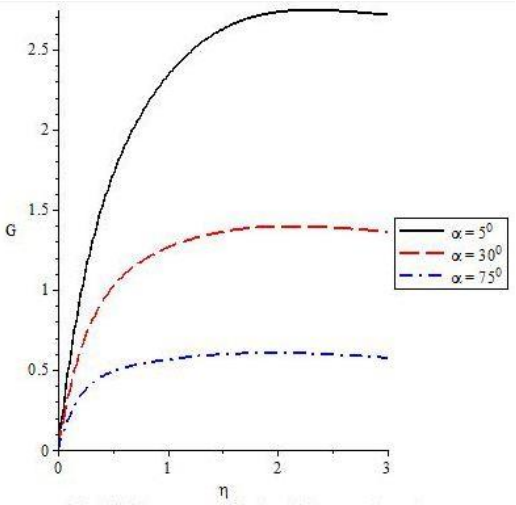

Figure 5: Pressure profile at a diverse angle

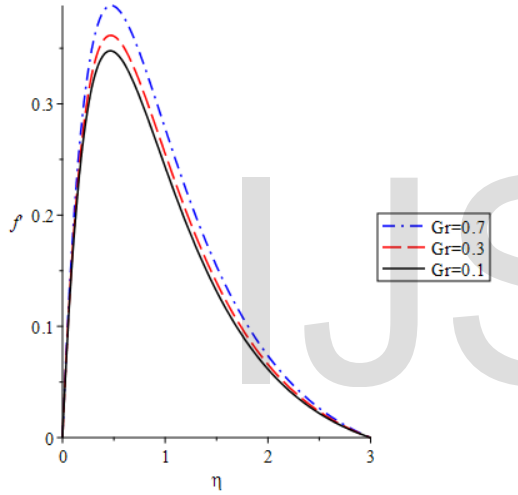

Figure 6: Effect of Gr on the flow rate

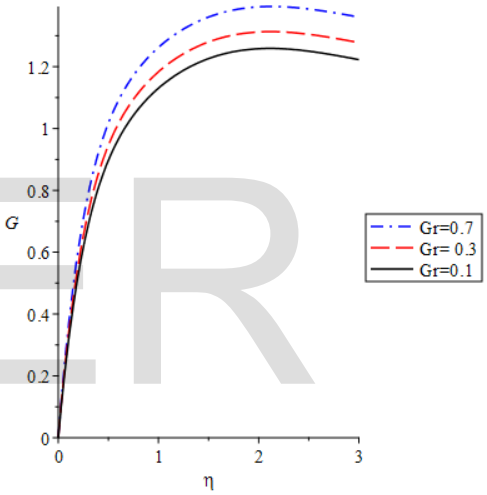

Figure 7: Influence of Gr on the pressure

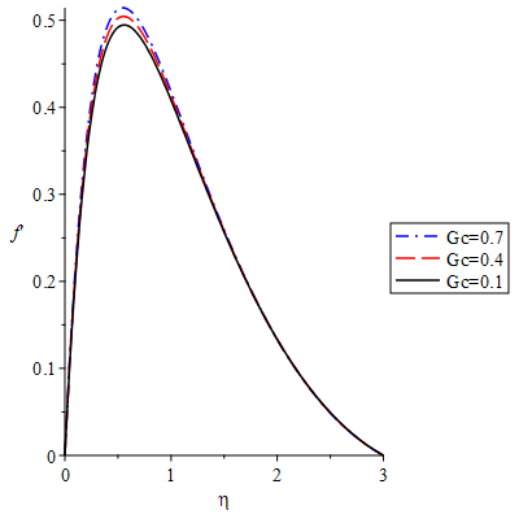

Figure 8: Velocity profile for various Gc

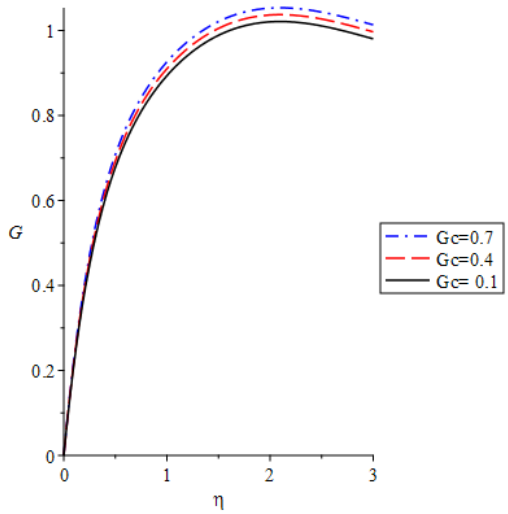

Figure 9: Gc impact on the pressure field

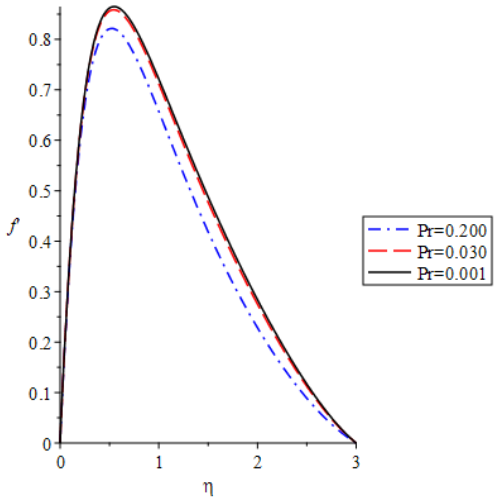

Figure 10: Flow velocity field for diverse Pr

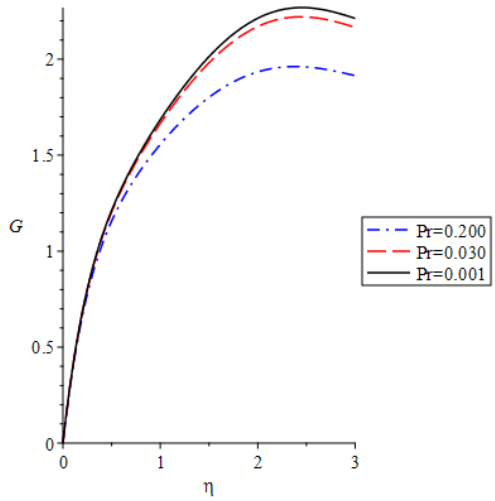

Figure 11: Pressure distribution for rising Pr

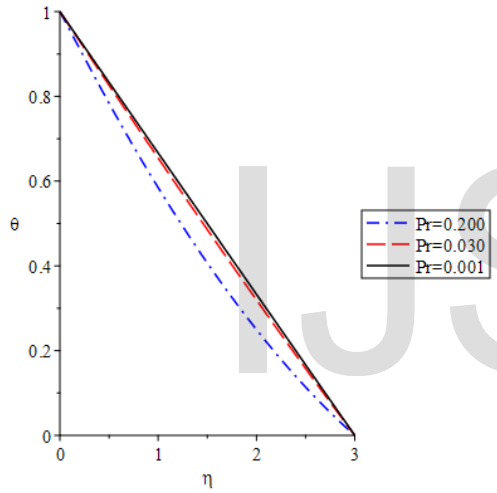

Figure 12: Temperature field for various Pr

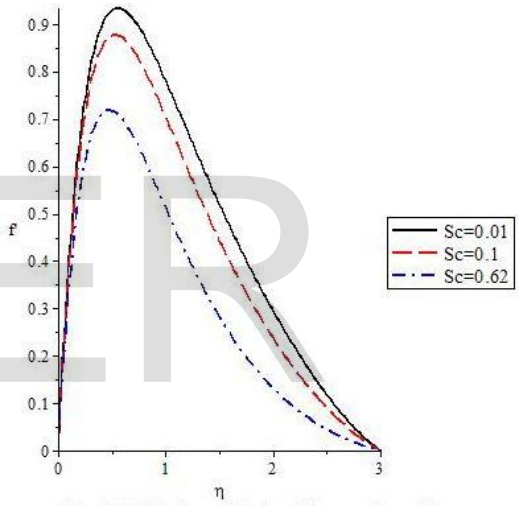

Figure 13: Flow rate field for different Sc

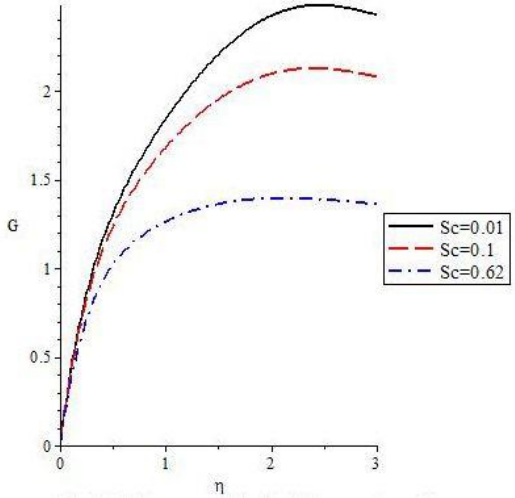

Figure 14: Pressure profile for rising Sc

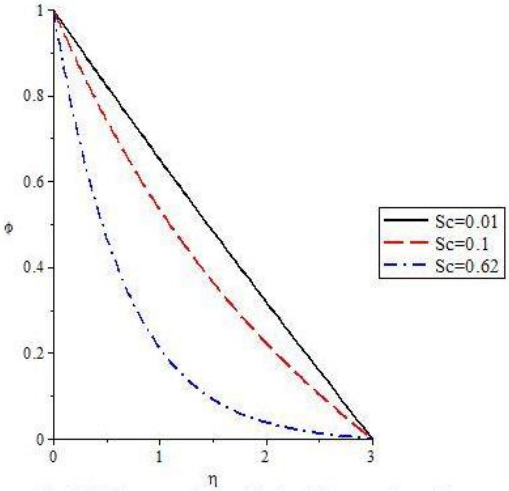

Figure 15: Mass distribution for rising Sc

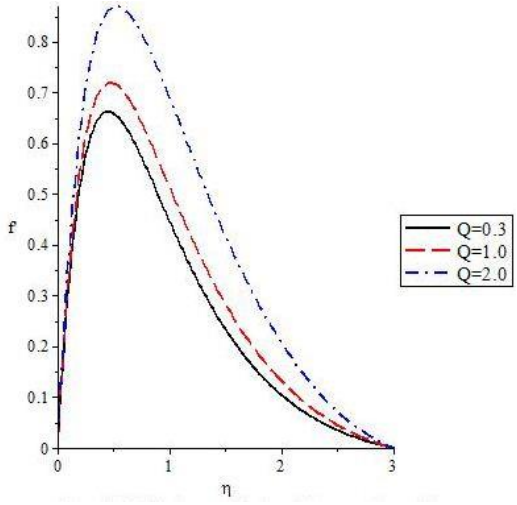

Figure 16: Impact of rising Q on the flow rate

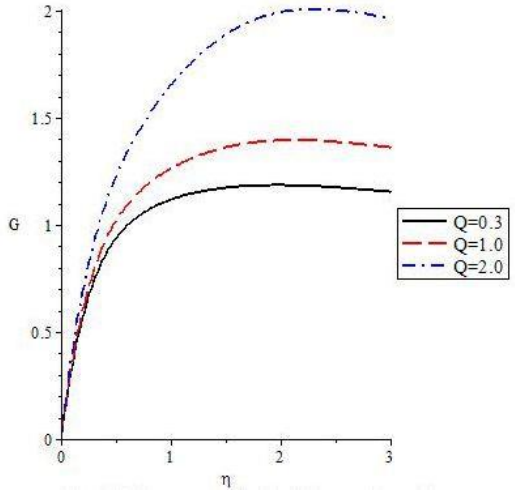

Figure 17: Effect of Q on the pressure field

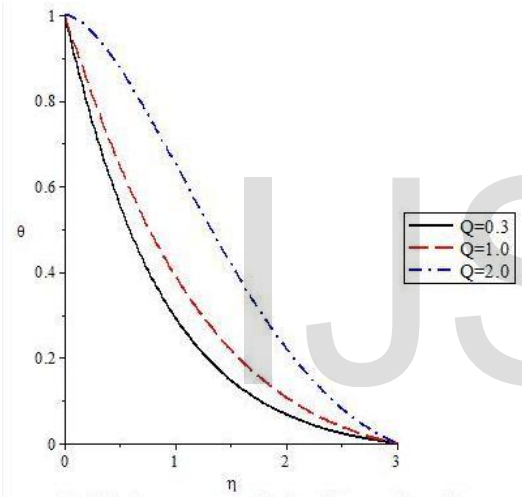

Figure 18: Temperature distribution for Q

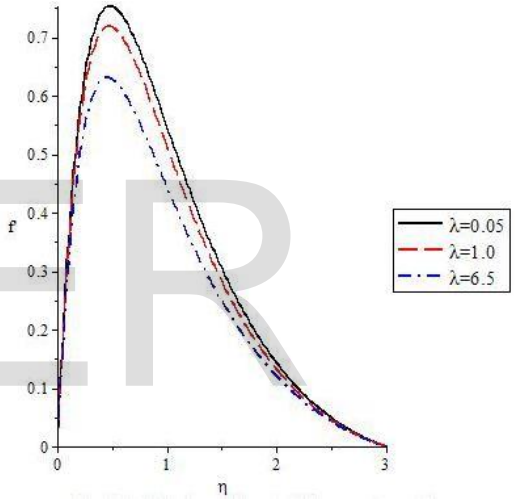

Figure 19: Influence of λ on the velocity field

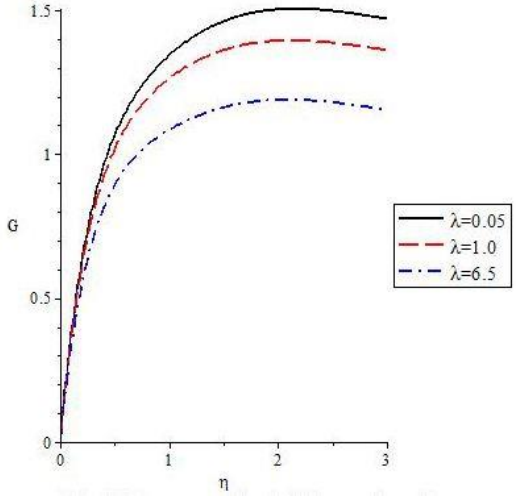

Figure 20: Changes in pressure for rising λ

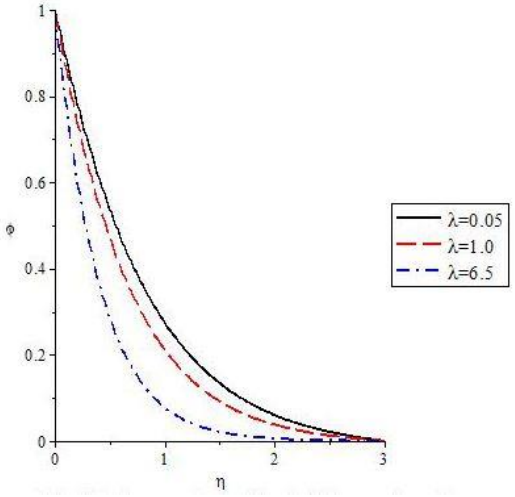

Figure 21: Concentration field for diverse λ

Conclusion

The partial differential equations of the fluid flow problem are non-dimensional and reduced to a couple of ordinary differential equations using scaling translational symmetries. The numerical solution for scaling symmetry is obtained using the Weighted Residual Method. From the numerical results, it is observed that an increase in the magnetic field parameter Hartmann or degree of inclination of the magnetic field is manifested as a decrease in the flow velocity and pressure profiles. The velocity and pressure distributions accelerate as the thermal Grashof or solutal Grashof numbers increases. In the presence of increasing Prandtl or Schmidt numbers, there is a corresponding decrease in velocity, pressure-temperature, or concentration profile. The velocity, pressure, and temperature distributions are seen to increase gradually as the heat source increases. Increasing the chemical reaction rate reduces the velocity, pressure, and concentration distributions.

References

[1] Salawu, S.O., Dada, M.S. (2016). Radiative heat transfer of variable viscosity and thermal conductivity effects on the inclined magnetic field with dissipation in a non-Darcy medium. Journal of the Nigerian Mathematical Society, 35, 93-106.

[2] Kareem, R.A., Salawu, S.O., Gbadeyan, J.A. (2018). Numerical analysis of non-uniform heat source/sink in a radiative micropolar variable electric conductivity fluid with dissipation Joule heating. American Journal of Applied Mathematics, 6(2), 34-41.

[3] Hassan, A.R., Salawu, S.O. (2019). Analysis of buoyancy-driven flow of a reactive heat-generating third-grade fluid in a parallel channel having convective boundary conditions. SN Applied Sciences, 1(8), 919.

[4] Youssef, Z.B., Mina, B.A., Nagwa, A.B., and Hossam, S.H. (2007). Lie-group method solution for two-dimensional viscous flow between slowly expanding or contracting walls with weak permeability. Applied Mathematical Modelling, 31(2007), 1092-1108.

[5] Mohammad, M.R., Esmaeel, E., and Behnam, R. (2014). Optimal homotopy asymptotic method for solving viscous flow through expanding or contracting gaps with permeable walls. Transaction on IoT and Cloud Computing, 2(1), 76-100.

[6] Manyonge, W.A., Kiema, D.W., and Iyaya, C.C. (2012). Steady MHD Poiseuille flow between two infinite parallel porous plates in an inclined magnetic field. International Journal of Pure and Applied Mathematics, 76(5), 661-668.

[7] Pramanik, S. (2013). Applications of scaling group of transformations to the boundary layer flow of a non-newtonian power-law fluid. Int. journal of Appl. Math and Mech., 9(6), 1-13.

[8] Makinde, O.D. (2010). On MHD heat and mass transfer over a moving vertical plate with a convective surface boundary condition. The Canadian Journal of Chemical Engineering, 9999, 700-710.

[9] Salawu S.O. and Amoo S.A. (2016). Effects of variable viscosity and thermal conductivity on dissipative heat and mass transfer of MHD flow in a porous medium. AIMS Research Journal, 2(2), 111-122

[10] Uwanta, I.J., and Sarki, M.N. (2012). Heat and mass transfer with variable temperature and exponential mass diffusion. International Journal Of Computational Engineering Research 2(5), 1487-1494.

[11] Alireza, R., Mahmood, F., and Seyed, R.V. (2013). Analytical solution for MHD stagnation point flow and heat transfer over a permeable stretching sheet with chemical reaction. Journal of Theoretical and Applied Mechanics, 51(3), 675-686.

[12] Okedoye, A.M., Salawu, S.O. (2019): Unsteady oscillatory MHD boundary layer flow past a moving plate with mass transfer and binary chemical reaction. SN Applied Sciences, 1(9), 1586.
[13] Hossain, M.S., Samand, M.A. (2013). Heat and mass transfer of MHD free convection flow along with a stretching sheet with chemical reaction, radiation, and heat generation in presence of a magnetic field. Research Journal of Mathematics and Statistics, 5(1-2), 05-17.
[14] Reddy, M.G. (2013). Scaling transformation for heat and mass transfer effects on steady MHD free convection dissipative flow past an inclined porous surface. Int. journal of Appl. Math. and Mech., 9(10), 1-18.
[15] Fatunmbi, E.O., and Fenuga, O.J. (2017). MHD micropolar fluid flow over a permeable stretching sheet in the presence of variable viscosity and thermal conductivity with Soret and Dufour effects. IJMAO, 17, 211- 232.
[16] Adeniyan, A., and Adigun, J.A. (2018). Stress-work and chemical reaction effects on MHD forced convection heat and mass transfer slip-flow towards a convectively heated plate in a non-Darcian porous medium with surface mass-flux, IJMAO, 18, 338-355.
[17] Salawu, S.O., Dada, M.S., Adebimpe, O. (2019): Analysis of pressure-driven heat and mass transfer of hydromagnetic flow past Darcy-Forchheimer porous media using Lie group. Journal of Engineering and Applied Science, 14(13), 4405-4413.
[18] Sayed-Ahmed, M.E., Hazem A.A., and Karem M.E. (2011). Time-dependent pressure gradient effect on unsteady MHD Couette flow and heat transfer of a Casson fluid. Scientific Research, 3(2011), 38-49.
[19] Farooq, M., Rahim, M.T., Islam, S., and Siddiqui, A.M. (2013). Steady Poiseuille flow and heat transfer couple stress fluids between two parallel inclined plates with variable viscosity. Journal of the Association of Arab Universities for Basic and Applied science, 14, 9-18.
[20] Thiagarajan, M., and Sangeetha, A.S. (2013). Nonlinear MHD boundary layer flow and heat transfer past a stretching plate with free stream pressure gradient in presence of variable viscosity and thermal conductivity. United States of America Research Journal, 1(4), 25-31.
[21] Mukhopadhyay, S., Layek, G.C., and Samad, S.A. (2005). Study of MHD boundary layer flow over a heated stretching sheet with variable viscosity. Int. J. Heat Mass Transfer 48, 60-66.
[22] Bhattacharyya, K., Uddin, M.S., and Layek, G.C. (2011). Application of scaling group of transformations to steady boundary layer flow of Newtonian fluid over a stretching sheet in presence of chemically reactive species. Journal of Bangladesh Academy of Sciences, 35(1), 43-50.
[23] Dada, M.S., and Salawu, S.O. (2017). Analysis of heat and mass transfer of an inclined magnetic field pressure-driven flow past a permeable plate. Applications and Applied Mathematics: An International Journal, 12(1), 189-200.
[24] McGrattan E.R. (1998). Application of weighted residual methods to dynamic economics models. Federal Reserve Bank of Minneapolis Research Department Staff Report 232.
[25] Odejide, S.A., and Aregbesola, Y.A.S. (2011). Applications of the method of weighted residuals to problems with a semi-finite domain. Rom. Journ. Phys., 56(1-2), 14-24.
[26] Salawu, S.O., Kareem, R.A. (2019). Analysis of heat absorption viscoelastic exothermic chemical reactive fluid with temperature-dependent viscosity under bimolecular kinetic. Applications and Applied Mathematics: An International Journal, 14(2), 1232-1242.